Detections for Ambient Backscatter Communications Systems with Dynamic Sources

Jixiang Chen, Quansheng Guan, *Senior Member, IEEE*, Yue Rong, *Senior Member, IEEE*, Hua Yu, *Member, IEEE*

***Abstract*—In this paper, signal detection in ambient backscatter communication (AmBC) with dynamic sources is investigated. Dynamic ambient radio frequency sources are the sources which transmit their signals randomly. The states of the dynamic source include the on-state and off-state. In the off-state, dynamic sources do not transmit any signal and the backscatter device cannot backscatter any signal accordingly. The received signals may contain only pure noises. Thus, it brings new challenges to the signal detection. We develop detection methods with/without truncating received signals for AmBC under both dynamic complex Gaussian source signals and dynamic M-ary phase-shift keying (M-PSK) source signals with on-off keying. To make detection simple and tractable for the dynamic M-PSK at the receiver, Manchester code is applied. Simulation results show it is necessary to truncate part of the signal in detections in the high signal-to-noise ratio region unless the received signals contain few pure noise samples, in order to reduce the bit-error-rate of backscatter signals.**

***Index Terms*—Ambient backscatter, dynamic sources, detection, truncated probability distribution function.**

I. Introduction

The ambient backscatter communication (AmBC) [1]–[4] technology has drawn growing interest from both academia and industry due to its low power consumption and spectrum sharing characteristics. In an AmBC system, the backscatter device relies on modulated ambient radio frequency (RF) signals rather than unmodulated dedicated ones. The ambient RF sources can be divided into two types, i.e., static ambient RF sources and dynamic ambient RF sources. Static ambient RF sources are the sources which transmit RF signals constantly, e.g., TV towers [5] and FM base stations [6]. Dynamic ambient RF sources refer to sources which operate randomly, e.g., Wi-Fi, mobile or radar system [7].

Existing works [8]–[24] mainly focus on studying the AmBC system under static sources while a few works explore the AmBC system under dynamic sources. The Guardrider system in [25] applies Reed-Solomon code to recover lost bits caused by the silent Wi-Fi signal. The authors in [26] assume the ambient source to have a Bernoulli distribution and investigate its channel capacity. While the capacity of AmBC with dynamic complex Gaussian source is reported in [27]. The work on signal detection and theoretical performance analysis of AmBC with dynamic sources is still scarce. The paper [7] explores the effect of the source signal on the detection performance assuming the source signal appears or disappears only once during the backscattering. However, a general source traffic model has not been explored.

The states of a dynamic source include the on-state and off-state, and the transition between the two states is random. In the on-state, the source transmits RF signals to serve its users. In the off-state, no RF signal is transmitted by the source. If the dynamic RF source is in the off-state, the backscatter device (BD) cannot reflect any signal and the signals sampled at the receiver are pure noises. In this sense, the BD should not transmit information to the receiver when the source is in the off-state. However, it is impossible for a passive tag to sense every state of the dynamic source since the ambient signals change rapidly. Consequently, the BD cannot backscatter the source signal only in the on-state. That is, the BD and the receiver cannot communicate only using the on-state parts of the dynamic source.

Without exactly tracking the source's states, the BD has to transmit its information continuously. If the BD uses dynamic sources to transmit its information, there must exist some time slots where the BD cannot backscatter any signal to the receiver. The received signals at the receiver contain not only backscattered signals but also the pure noise signal which is useless and imposes a huge challenge to the signal detection for AmBC.

To deal with this problem, the receiver should find these pure noise samples and discard them. However, these pure noises are not easy to be removed/truncated completely from received signals because the receiver does not have the exact source state information and pure noises are mixed with other information signals. If the truncation threshold is too low, the pure noises cannot be discarded. On the other hand, some information signals will also be removed with a high truncation threshold. We need to determine an appropriate truncation threshold for the receiver. Moreover, if the noise signal is large enough, the useful signal can also be abandoned by the truncation threshold. In this situation, the necessity of the truncation at the receiver remains unknown. Thus, both two detection cases with or without truncation threshold should be explored to handle different communication scenarios.

In this paper, we investigate the signal detection of AmBC with dynamic sources. First, the on-off keying (OOK) modula-

This work was supported by the National Natural Science Foundation of China under Grants U23A20281, 62341129 and 62192712, and the Science and Technology Planning Project of Guangdong Province of China under Grant 2023A0505050097.

Jixiang Chen, Quansheng Guan, and Hua Yu are with the School of Electronic and Information Engineering, South China University of Technology, Guangzhou 510640, China, are also with the Key Laboratory of Marine Environmental Survey Technology and Application, Ministry of Natural Resources, Guangzhou 510300, China (Corresponding author: Quansheng Guan; e-mail: eejxchen@mail.scut.edu.cn; eeqshguan@scut.edu.cn; yuhua@scut.edu.cn).

Y. Rong is with the School of Electrical Engineering, Computing and Mathematical Sciences, Curtin University, Bentley, WA 6102, Australia (e-mail: y.rong@curtin.edu.au).

tion is adopted at the tag. We study the two cases of truncating the noise and not. The receiver can exclude part of the received signal with a truncation threshold. To this end, first, the truncation threshold should be determined. Then, the receiver detects the backscatter symbol from the residual signals. It is challenging to detect the backscattered symbols under dynamic sources because received signals with or without truncation are more complicated than the received signals under static sources.

Second, to make the detection operation simple and tractable for the dynamic M-ary phase-shift keying (M-PSK) source at the receiver, we propose that the tag uses Manchester code to backscatter the dynamic source signal. Manchester code is a line code in which the encoding of each data bit is either low then high, or high then low, for equal time. With Manchester code, the detecting threshold is not required since we can detect the backscattered symbol by simply comparing the two energy levels. The energy truncation threshold does not need to be calculated, as the signal truncation can be done by simply throwing away the same number of received signals of the first and second half part in Manchester code. Instead, only the number of truncated received signals is required.

Our contributions are summarized as follows:

- Detections for ambient backscatter communication with dynamic complex Gaussian (CG) and M-PSK sources with the OOK modulation are investigated. Both the likelihood ratio test (LRT) detector and the energy detector (ED) with truncated or not truncated received signal for the dynamic CG source are developed. Besides, the energy detector for the dynamic M-PSK source is studied. The corresponding approximated bit-error-rates (BERs) for ED based methods are derived in closed form when the ratio of the duration of one backscattered symbol to the duration of one ambient source symbol is large.
- Detections for Manchester coded AmBC system under dynamic CG and M-PSK sources are explored. For both two sources, ED and truncated ED (TED) are presented. Moreover, tractable BER expressions are derived in closed form.
- Numerical results show the detector with truncated received signals achieves a better BER performance than the detector with all received signals in the high signal-to-noise ratio (SNR) region unless there are few pure noise samples in received signals.

The remainder of this paper is organized as follows. Section II describes the channel model and signal model for AmBC with dynamic sources. In Section III, the detection methods for the OOK modulation are developed. In Section IV the detection methods of Manchester code are investigated. Simulation results are provided in Section V. Finally, Section VI concludes this paper.

Notations: Scalars are lowercase letters, while vectors and matrices are boldfaced letters. $\mathbf{0}_{\mathrm{m\times n}}$ and $\mathbf{1}_{\mathrm{m\times n}}$ represent respectively $m \times n$ all zero and all one matrices. $\mathcal{N}(\mu, \sigma^2)$ and $\mathcal{CN}(\mu, \sigma^2)$ denote the real Gaussian and complex Gaussian distribution with mean μ and variance σ^2, respectively. The function $erfc(x) = \frac{2}{\sqrt{\pi}} \int_x^{+\infty} e^{-t^2} dt$ returns the complementary error function evaluated at x. $E[x]$ and $Var[x]$ represent respectively the mean and variance of x. The function $Q(x) = \int_x^{+\infty} \frac{1}{\sqrt{2\pi}} exp(-\frac{t^2}{2}) dt$ is the tail distribution function of the standard normal distribution.

II. System Model

A. Wireless Channel Model

Consider an ambient backscatter communication system consisting of an ambient source, a tag and a reader as in Fig. 1. Each of them is equipped with a single antenna. We denote the channel from the source to the reader as a direct channel h_d, the channel from the source to the tag as a forward channel h_f, and the channel from the tag to the reader as a backward channel h_b, respectively. We assume that AmBC channels obey a frequency-flat and block-fading channel model, where all the channels keep unchanged within the channel coherence time but may vary in different coherence intervals independently.

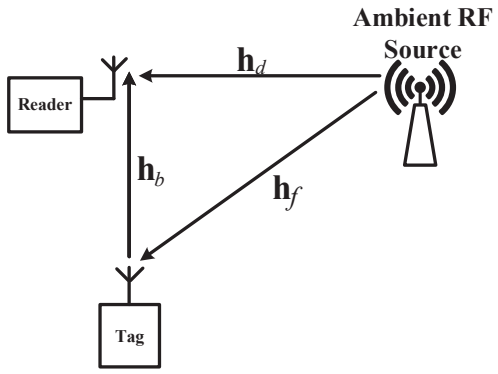

Fig. 1. System model of ambient backscatter communications.

B. Signal Model

With different impedance, the tag can vary the amount of signals backscattered to the reader. Taking binary amplitude-shift keying modulation as an example, if the tag wants to transmit '0', it will adjust its impedance so that little of the incident signal is backscattered; while if the tag wants to transmit '1', all of the incident signal will be backscattered to the reader.

The ambient dynamic source broadcasts its signal to the air, which can be received by both the tag and the reader. Denote the backscattered signal of tag as $x(n) \in \{0, 1\}$ and the source signal as $s(n)$. The received signal at the reader is

$$y(n) = h_d s(n) + h_b h_f \alpha x(n) s(n) + w(n), \tag{1}$$

where α is a coefficient representing the scattering efficiency and antenna gain, $w(n)$ is the zero-mean additive white Gaussian noise (AWGN) with variance σ_w^2. Let $h_0 = h_d$ and $h_1 = h_d + h_b h_f \alpha$ for notation simplicity, we get

$$y(n) = \begin{cases} h_0 s(n) + w(n), x(n) = 0, \\ h_1 s(n) + w(n), x(n) = 1. \end{cases} \tag{2}$$

In this paper, we assume that perfect channel energy information $|h_1|^2$ and $|h_0|^2$ are known at the receiver to investigate its optimal detection performance.

Since backscattered signals are weak compared to the source signals, the duration of the backscatter symbol is normally N (an even number without loss of generality) times the duration of the source symbol. The received signal corresponding to a backscatter symbol is $\boldsymbol{y} = [y(1), y(2), \cdots, y(N)]$. If the OOK modulation is used at the tag, the uncoded transmission symbols vector $\boldsymbol{x} = [x(1), x(2), \cdots, x(N)]$ is chosen from $\{\mathbf{0}_{1\times \mathrm{N}}, \mathbf{1}_{1\times \mathrm{N}}\}$. The transmission symbols vector $\boldsymbol{x}$ belongs to $\{\mathbf{1}_{1\times \mathrm{N}/2}\mathbf{0}_{1\times \mathrm{N}/2}, \mathbf{0}_{1\times \mathrm{N}/2}\mathbf{1}_{1\times \mathrm{N}/2}\}$ if Manchester code is applied at the tag.

It is possible that the source is off within the duration of one backscatter symbol, and pure noise is received at the receiver. In this paper, we consider the off part would not happen to a whole backscatter symbol. The Wi-Fi system follows CSMA/CA with inter-frame space, backoff and fragmentation. Inter-frame space and backoff are short and random, which make the source signal off. Fragmentation is adopted to reduce the probability of packet collision. The maximum frame duration is $542\mu s$ for IEEE 802.11g [25]. Then, if the duration of the tag symbol is $1000\mu s$ (the rate is 1 kbps as adopted in two fundamental works in [5], [29]), the state of the source will have multiple transitions between on and off during one backscatter symbol.

We consider that the source period is smaller than the tag frame. Specifically, we consider that the source period is smaller than one backscatter symbol. In this case, the probability of losing an entire frame or most of the symbols in a frame is close to zero. If backscatter symbols can be recovered by detection techniques, retransmission will be unnecessary.

The probability of the on-state and off-state of the source are z_{on} and z_{off} respectively, and $z_{on} + z_{off} = 1$. Assume that z_{on} and z_{off} are known at the receiver. The transition between the on-state and off-state is assumed to be independent. In this paper, we consider two types of dynamic sources including dynamic CG sources and dynamic M-PSK sources. To facilitate the detection in the sequel, some probability density functions (PDFs) of the received signal are required.

Case 1: In the case of dynamic CG sources, we assume the source signal to be CG distributed with zero mean when the source is in the on-state, i.e., $s_{on}(n) \sim \mathcal{CN}(0, \sigma_s^2)$. Otherwise, the source signal is in the off-state, i.e., $s_{off}(n) = 0$. This case is practical since Wi-Fi signals are modulated by orthogonal frequency-division multiplexing (OFDM) modulated. Its time domain signal is modelled as Gaussian signals [7]. Also, in a practical radio environment, the source could be a sum of many random signals and according to the central limit theorem, the overall signal can be approximated as Gaussian [7].

The PDF of $y(n)$ can be derived as

$$y(n) \sim \begin{cases} \mathcal{CN}(0, \sigma_1^2), x(n) = 1, s(n) = s_{on}(n), \\ \mathcal{CN}(0, \sigma_0^2), x(n) = 0, s(n) = s_{on}(n), \\ \mathcal{CN}(0, \sigma_w^2), x(n) = 1, s(n) = s_{off}(n), \\ \mathcal{CN}(0, \sigma_w^2), x(n) = 0, s(n) = s_{off}(n), \end{cases} \tag{3}$$

where $\sigma_0^2 = |h_0|^2\sigma_s^2 + \sigma_w^2$ and $\sigma_1^2 = |h_1|^2\sigma_s^2 + \sigma_w^2$. In summary, the probability of $y(n)$ conditioned on $x = 1$ and $x = 0$ are

$$p(y(n)|x = 1) = \frac{z_{on}}{\pi\sigma_1^2} e^{-\frac{|y(n)|^2}{\sigma_1^2}} + \frac{z_{off}}{\pi\sigma_w^2} e^{-\frac{|y(n)|^2}{\sigma_w^2}}, \tag{4}$$

$$p(y(n)|x = 0) = \frac{z_{on}}{\pi\sigma_0^2} e^{-\frac{|y(n)|^2}{\sigma_0^2}} + \frac{z_{off}}{\pi\sigma_w^2} e^{-\frac{|y(n)|^2}{\sigma_w^2}}. \tag{5}$$

The probability of $\boldsymbol{y}$ conditioned on $x = i$ with respect to the OOK modulation is

$$p(\boldsymbol{y}|x=i) = \prod_{n=1}^{N} \left(z_{on} \frac{1}{\pi\sigma_i^2} e^{-\frac{|y(n)|^2}{\sigma_i^2}} + z_{off} \frac{1}{\pi\sigma_w^2} e^{-\frac{|y(n)|^2}{\sigma_w^2}} \right). \tag{6}$$

As for the energy $r(n) = |y(n)|^2$, it is subject to

$$r(n) \sim \begin{cases} \frac{1}{\sigma_1^2} e^{-\frac{r(n)}{\sigma_1^2}}, x(n) = 1, s(n) = s_{on}(n), \\ \frac{1}{\sigma_0^2} e^{-\frac{r(n)}{\sigma_0^2}}, x(n) = 0, s(n) = s_{on}(n), \\ \frac{1}{\sigma_w^2} e^{-\frac{r(n)}{\sigma_w^2}}, x(n) = 1, s(n) = s_{off}(n), \\ \frac{1}{\sigma_w^2} e^{-\frac{r(n)}{\sigma_w^2}}, x(n) = 0, s(n) = s_{off}(n). \end{cases} \tag{7}$$

Using (7), the probability of $r(n)$ conditioned on $x = i$ can be rewritten as

$$p(r(n)|x = i) = \frac{z_{on}}{\sigma_i^2} e^{-\frac{r(n)}{\sigma_i^2}} + \frac{z_{off}}{\sigma_w^2} e^{-\frac{r(n)}{\sigma_w^2}}. \tag{8}$$

Case 2: In the case of the dynamic M-PSK source signal, this source signal can be expressed as

$$\begin{cases} s_{on}(n) \in \{\sqrt{P_s} e^{\frac{2\pi j(m-1)}{M}}\}, m = 1, \cdots M, \\ s_{off}(n) = 0, \end{cases} \tag{9}$$

where P_s is average signal power of $s_{on}(n)$. The PDF of $y(n)$ conditioned on $x = i$ is

$$\begin{aligned} p(y(n)|x = i) =& z_{on} \left(\sum_{m=1}^{M} \frac{\lambda_m}{\pi\sigma_w^2} e^{-\frac{\left| y(n) - h_i\sqrt{P_s} e^{\frac{2\pi j(m-1)}{M}} \right|^2}{\sigma_w^2}} \right) \\ &+ z_{off} \frac{1}{\pi\sigma_w^2} e^{-\frac{|y(n)|^2}{\sigma_w^2}}, \end{aligned} \tag{10}$$

where λ_m is the probability of the m-th PSK symbol. Assume that these PSK symbols are sent with equal probabilities. That is, $\lambda_m = 1/M$. Correspondingly, the joint PDF of $\mathbf{y}$ with regard to the OOK modulation is shown as follows

$$\begin{aligned} p(\boldsymbol{y}|x=i) = \prod_{n=1}^{N} \Bigg[& z_{on} \left(\sum_{m=1}^{M} \frac{\lambda_m}{\pi\sigma_w^2} e^{-\frac{\left| y(n) - h_i\sqrt{P_s} e^{\frac{2\pi j(m-1)}{M}} \right|^2}{\sigma_w^2}} \right) \\ &+ z_{off} \frac{1}{\pi\sigma_w^2} e^{-\frac{|y(n)|^2}{\sigma_w^2}} \Bigg]. \end{aligned} \tag{11}$$

III. OOK Modulation and Detection

In this section, the OOK modulation is adopted at the tag to backscatter the dynamic source signal. We will study the

LRT detection and the ED with or without truncated received signals for the dynamic CG signal. Then, ED for the dynamic M-PSK source signal is presented.

A. LRT Detection with Dynamic CG Source

Under the maximum likelihood (ML) principle, the backscatter symbol detection can be achieved from an LRT, defined as

$$\frac{p(\boldsymbol{y}|\mathcal{H}_1)}{p(\boldsymbol{y}|\mathcal{H}_0)} \underset{\mathcal{H}_0}{\overset{\mathcal{H}_1}{\gtrless}} 1, \tag{12}$$

where $\mathcal{H}_0$ denotes the hypothesis of $x(n) = 0$ and $\mathcal{H}_1$ denotes the hypothesis of $x(n) = 1$.

Substituting (6) into (12), the backscattered symbol can be detected by

$$\frac{\prod_{n=1}^{N}\left(z_{on}\frac{1}{\pi\sigma_1^2}e^{-\frac{|y(n)|^2}{\sigma_1^2}} + z_{off}\frac{1}{\pi\sigma_w^2}e^{-\frac{|y(n)|^2}{\sigma_w^2}}\right)}{\prod_{n=1}^{N}\left(z_{on}\frac{1}{\pi\sigma_0^2}e^{-\frac{|y(n)|^2}{\sigma_0^2}} + z_{off}\frac{1}{\pi\sigma_w^2}e^{-\frac{|y(n)|^2}{\sigma_w^2}}\right)} \underset{\mathcal{H}_0}{\overset{\mathcal{H}_1}{\gtrless}} 1. \tag{13}$$

Due to the complexity of $p(\boldsymbol{y}|x = i)$ in (6), it is intractable to derive a closed-form expression for the BER based on (13).

B. Truncated Likelihood Ratio Test (TLRT) Detection with Dynamic CG Source

To investigate whether the TLRT detection can achieve a better performance than the LRT detection, the TLRT detection is also studied.

To truncate the noise signal, the truncation threshold should be obtained first. We need to use the truncation threshold to distinguish the noise signal and useful signals. There are three types of the received signal including pure noises, the backscattered signal plus the source signal plus noise, and the source signal plus noise. The power of the superposition of the source and the backscattered signals for $x(n) = 1$ is not guaranteed larger than that of the signals for $x(n) = 0$ because the channel coefficients and signals are complex. Thus, there are two cases when determining the truncation threshold as shown in (14).

Denote $\mathcal{H}_{on}$ and $\mathcal{H}_{off}$ as the hypotheses that the source is in the on-state and the off-state. Using the ML principle, the state of the source can be estimated by

$$\begin{aligned}\frac{p(y(n)|\mathcal{H}_{on},\mathcal{H}_0)}{p(y(n)|\mathcal{H}_{off},\mathcal{H}_1)} &\underset{\mathcal{H}_{off}}{\overset{\mathcal{H}_{on}}{\gtrless}} 1, \sigma_1^2 > \sigma_0^2,\\ \frac{p(y(n)|\mathcal{H}_{on},\mathcal{H}_1)}{p(y(n)|\mathcal{H}_{off},\mathcal{H}_1)} &\underset{\mathcal{H}_{off}}{\overset{\mathcal{H}_{on}}{\gtrless}} 1, \sigma_1^2 < \sigma_0^2.\end{aligned} \tag{14}$$

Substituting (3) into (14), (14) is simplified to

$$|y(n)|^2 \underset{\mathcal{H}_{off}}{\overset{\mathcal{H}_{on}}{\gtrless}} T_s, \tag{15}$$

where

$$\begin{aligned}T_s &= \ln\left(\frac{\sigma_0^2}{\sigma_w^2}\right)\frac{\sigma_0^2\sigma_w^2}{\sigma_0^2-\sigma_w^2}, \sigma_1^2 > \sigma_0^2,\\ T_s &= \ln\left(\frac{\sigma_1^2}{\sigma_w^2}\right)\frac{\sigma_1^2\sigma_w^2}{\sigma_1^2-\sigma_w^2}, \sigma_1^2 < \sigma_0^2,\end{aligned} \tag{16}$$

is the optimal source state detection threshold.

Denote the signals after truncation as $y_t(n), n = 1, 2, \cdots, N_{on,i}, i = 0, 1$. The PDF of $y_t(n)$ is calculated by [30], [31]

$$\begin{aligned}p(y_t(n)|x = i) &= \frac{p(y(n)|x = i)|y = y_t(n)}{\int_{\sqrt{T_s}}^{+\infty} p(y(n)|x = i)dy(n)}\\ &= \frac{\frac{z_{on}}{\sigma_i^2}e^{-\frac{r_t(n)}{\sigma_i^2}} + \frac{z_{off}}{\sigma_w^2}e^{-\frac{r_t(n)}{\sigma_w^2}}}{z_{on}e^{-\frac{T_s}{\sigma_i^2}} + z_{off}e^{-\frac{T_s}{\sigma_w^2}}}, |y_t(n)| > \sqrt{T_s},\end{aligned} \tag{17}$$

where $r_t(n) = |y_t(n)|^2$.

The joint PDF of the truncated signals is

$$p(\boldsymbol{y_t}|x = i) = \prod_{n=1}^{N_{on,i}}\left[\frac{\frac{z_{on}}{\sigma_i^2}e^{-\frac{r_t(n)}{\sigma_i^2}} + \frac{z_{off}}{\sigma_w^2}e^{-\frac{r_t(n)}{\sigma_w^2}}}{z_{on}e^{-\frac{T_s}{\sigma_i^2}} + z_{off}e^{-\frac{T_s}{\sigma_w^2}}}\right], \tag{18}$$

where $\boldsymbol{y_t} = [y_t(1), y_t(2), \cdots, y_t(N_{on,i})]$. Thus, the LRT detection can be written as

$$\frac{p(\boldsymbol{y_t}|\mathcal{H}_1)}{p(\boldsymbol{y_t}|\mathcal{H}_0)} = \frac{\prod_{n=1}^{N_{on,1}}\left[\frac{\frac{z_{on}}{\sigma_1^2}e^{-\frac{r_t(n)}{\sigma_1^2}} + \frac{z_{off}}{\sigma_w^2}e^{-\frac{r_t(n)}{\sigma_w^2}}}{z_{on}e^{-\frac{T_s}{\sigma_1^2}} + z_{off}e^{-\frac{T_s}{\sigma_w^2}}}\right]}{\prod_{n=1}^{N_{on,0}}\left[\frac{\frac{z_{on}}{\sigma_0^2}e^{-\frac{r_t(n)}{\sigma_0^2}} + \frac{z_{off}}{\sigma_w^2}e^{-\frac{r_t(n)}{\sigma_w^2}}}{z_{on}e^{-\frac{T_s}{\sigma_0^2}} + z_{off}e^{-\frac{T_s}{\sigma_w^2}}}\right]} \underset{\mathcal{H}_0}{\overset{\mathcal{H}_1}{\gtrless}} 1. \tag{19}$$

Due to its complexity, (19) cannot be further simplified and the corresponding closed-form BER expression is also intractable.

C. ED with Dynamic CG Source

To reduce the detection calculation complexity, the energy detection is applied to detect the backscattered symbol. Let $Z_{dcg,i} = \frac{1}{N}\sum_{n=1}^{N}\left|y(n)|_{x=i}\right|^2$.

Theorem 1: The PDF of the average energy $Z_{dcg,i}$ of $\boldsymbol{y}$ is approximated when N is large and derived as

$$Z_{dcg,i} \sim \mathcal{N}(\mu_{dcg,i}, \sigma_{dcg,i}^2), i = 0, 1, \tag{20}$$

where

$$\begin{aligned}\mu_{dcg,i} =& z_{on}\sigma_i^2 + z_{off}\sigma_w^2,\\ \sigma_{dcg,i}^2 =& \frac{2z_{on}\sigma_i^4 + 2z_{off}\sigma_w^4 - (z_{on}\sigma_i^2 + z_{off}\sigma_w^2)^2}{N}.\end{aligned} \tag{21}$$

Proof: The energy $Z_{dcg,i}$ is the average of the sum of N independent identically distribution (*i.i.d.*) signals. When N is large, it can be approximated by a Gaussian distribution. Its mean is the same as r and variance equals the variance of r

scaled by $1/N$. First, the mean of r is obtained by

$$\begin{aligned} E[r|x=i] &= \int_0^{+\infty} r f(r|x=i)dr \\ &= \int_0^{+\infty} r\left(\frac{z_{on}}{\sigma_i^2}e^{-\frac{r}{\sigma_i^2}} + \frac{z_{off}}{\sigma_w^2}e^{-\frac{r}{\sigma_w^2}}\right)dr \\ &= z_{on}\sigma_i^2 + z_{off}\sigma_w^2. \end{aligned} \tag{22}$$

Then, the mean of r^2 is calculated as

$$\begin{aligned} E[r^2|x=i] &= \int_0^{+\infty} r^2 f(r|x=i)dr \\ &= \int_0^{+\infty} r^2\left(\frac{z_{on}}{\sigma_i^2}e^{-\frac{r}{\sigma_i^2}} + \frac{z_{off}}{\sigma_w^2}e^{-\frac{r}{\sigma_w^2}}\right)dr \\ &= 2z_{on}\sigma_i^4 + 2z_{off}\sigma_w^4. \end{aligned} \tag{23}$$

Finally, the variance of r is

$$\begin{aligned} &Var[r|x=i] \\ =&E[r^2|x=i] - (E[r|x=i])^2 \\ =&2z_{on}\sigma_i^4 + 2z_{off}\sigma_w^4 - (z_{on}\sigma_i^2 + z_{off}\sigma_w^2)^2. \end{aligned} \tag{24}$$

Then, the mean and variance of $Z_{dcg,i}$ are given by (21). □

The detection threshold T_h^{dcg} can be computed from

$$f(Z_{dcg,1}|\mathcal{H}_1) = f(Z_{dcg,0}|\mathcal{H}_0). \tag{25}$$

That is,

$$\frac{1}{\sqrt{2\pi\sigma_{dcg,1}^2}}e^{-\frac{\left(T_h^{dcg}-\mu_{dcg,1}\right)^2}{2\sigma_{dcg,1}^2}} = \frac{1}{\sqrt{2\pi\sigma_{dcg,0}^2}}e^{-\frac{\left(T_h^{dcg}-\mu_{dcg,0}\right)^2}{2\sigma_{dcg,0}^2}}. \tag{26}$$

Taking the natural logarithm of both sides of (26) and rearranging the terms, we obtain

$$c_1(T_h^{dcg})^2 + c_2 T_h^{dcg} + c_3 = 0, \tag{27}$$

where $c_1 = \sigma_{dcg,0}^2 - \sigma_{dcg,1}^2$, $c_2 = 2(\mu_{dcg,0}\sigma_{dcg,1}^2 - \mu_{dcg,1}\sigma_{dcg,0}^2)$ and $c_3 = \mu_{dcg,1}^2\sigma_{dcg,0}^2 - \mu_{dcg,0}^2\sigma_{dcg,1}^2 - \sigma_{dcg,1}^2\sigma_{dcg,0}^2\ln\left(\frac{\sigma_{dcg,0}^2}{\sigma_{dcg,1}^2}\right)$. As T_h^{dcg} is the detection threshold of the received signal energy, only the positive root of (27) is valid, which gives the threshold T_h^{dcg}. The decision rule is

$$p(Z_{dcg,0}|\mathcal{H}_0) \underset{\mathcal{H}_1}{\overset{\mathcal{H}_0}{\gtrless}} p(Z_{dcg,1}|\mathcal{H}_1) \Longleftrightarrow \begin{cases} Z_{dcg} \underset{\mathcal{H}_1}{\overset{\mathcal{H}_0}{\lessgtr}} T_h^{dcg}, & \sigma_0^2 > \sigma_1^2, \\ Z_{dcg} \underset{\mathcal{H}_1}{\overset{\mathcal{H}_0}{\gtrless}} T_h^{dcg}, & \sigma_0^2 < \sigma_1^2. \end{cases} \tag{28}$$

If $\sigma_0^2 > \sigma_1^2$, the corresponding BER can be obtained by

$$\begin{aligned} P_b^{dcg} &= p(\mathcal{H}_0)p(Z_{dcg} < T_h^{dcg}|\mathcal{H}_0) \\ &\quad + p(\mathcal{H}_1)p(Z_{dcg} > T_h^{dcg}|\mathcal{H}_1) \\ &= \frac{1}{2}\int_{-\infty}^{T_h^{dcg}} p(Z_{dcg}|\mathcal{H}_0)dz + \frac{1}{2}\int_{T_h^{dcg}}^{+\infty} p(Z_{dcg}|\mathcal{H}_1)dz \\ &= \frac{1}{2} - \frac{1}{2}Q\left(\frac{T_h^{dcg}-\mu_{dcg,0}}{\sigma_{dcg,0}}\right) + \frac{1}{2}Q\left(\frac{T_h^{dcg}-\mu_{dcg,1}}{\sigma_{dcg,1}}\right). \end{aligned} \tag{29}$$

If $\sigma_0^2 < \sigma_1^2$, the BER is similarly derived as

$$P_b^{dcg} = \frac{1}{2} + \frac{1}{2}Q\left(\frac{T_h^{dcg}-\mu_{dcg,0}}{\sigma_{dcg,0}}\right) - \frac{1}{2}Q\left(\frac{T_h^{dcg}-\mu_{dcg,1}}{\sigma_{dcg,1}}\right). \tag{30}$$

D. TED with the Dynamic CG Source

The received signals are truncated by the threshold calculated in (16). The PDF of the energy of the signal after truncation is

$$\begin{aligned} &p(r_t = |y_t|^2|x=i) \\ &= \frac{p(r|x=i)|r=r_t}{\int_{T_s}^{+\infty} p(r|x=i)dr} \\ &= \frac{\frac{z_{on}}{\sigma_i^2}e^{-\frac{r_t}{\sigma_i^2}} + \frac{z_{off}}{\sigma_w^2}e^{-\frac{r_t}{\sigma_w^2}}}{\left(\frac{z_{on}}{\sigma_i^2}e^{-\frac{r}{\sigma_i^2}} + \frac{z_{off}}{\sigma_w^2}e^{-\frac{r}{\sigma_w^2}}\right)\Big|_{T_s}^{+\infty}} \\ &= \frac{\frac{z_{on}}{\sigma_i^2}e^{-\frac{r_t}{\sigma_i^2}} + \frac{z_{off}}{\sigma_w^2}e^{-\frac{r_t}{\sigma_w^2}}}{z_{on}e^{-\frac{T_s}{\sigma_i^2}} + z_{off}e^{-\frac{T_s}{\sigma_w^2}}}, r_t > T_s. \end{aligned} \tag{31}$$

The mean of r_t is

$$\begin{aligned} E[r_t|x=i] &= \int_{T_s}^{+\infty} r_t p(r_t|x=i)dr_t \\ &= \int_{T_s}^{+\infty} r_t \frac{\frac{z_{on}}{\sigma_i^2}e^{-\frac{r_t}{\sigma_i^2}} + \frac{z_{off}}{\sigma_w^2}e^{-\frac{r_t}{\sigma_w^2}}}{z_{on}e^{-\frac{T_s}{\sigma_i^2}} + z_{off}e^{-\frac{T_s}{\sigma_w^2}}}dr_t \\ &= \frac{z_{on}(T_s+\sigma_i^2)e^{-\frac{T_s}{\sigma_i^2}} + z_{off}(T_s+\sigma_w^2)e^{-\frac{T_s}{\sigma_w^2}}}{z_{on}e^{-\frac{T_s}{\sigma_i^2}} + z_{off}e^{-\frac{T_s}{\sigma_w^2}}}. \end{aligned} \tag{32}$$

The second-order moment of r_t is

$$\begin{aligned} E[{r_t}^2|x=i] &= \int_{T_s}^{+\infty} r_t^2 p(r_t|x=i)dr_t \\ &= \frac{z_{on}({T_s}^2 + 2T_s\sigma_1^2 + 2\sigma_1^4)e^{-\frac{T_s}{\sigma_1^2}}}{z_{on}e^{-\frac{T_s}{\sigma_1^2}} + z_{off}e^{-\frac{T_s}{\sigma_w^2}}} \\ &\quad + \frac{z_{off}({T_s}^2 + 2T_s\sigma_w^2 + 2\sigma_w^4)e^{-\frac{T_s}{\sigma_w^2}}}{z_{on}e^{-\frac{T_s}{\sigma_1^2}} + z_{off}e^{-\frac{T_s}{\sigma_w^2}}}. \end{aligned} \tag{33}$$

The variance of r_t can be obtained by

$$Var[r_t|x=i] = \mathrm{E}[{r_t}^2|x=i] - E[r_t|x=i]^2. \tag{34}$$

The average energy of the truncated received signals is

$$\begin{aligned} Z_{dcg,i}^t &= \frac{1}{N_{on,i}}\sum_{n=1}^{N_{on,i}} \left|y_t(n)|_{x=i}\right|^2 \\ &\sim \mathcal{N}(E[r_t|x=i], \frac{Var[r_t|x=i]}{N_{on,i}}). \end{aligned} \tag{35}$$

Following the similar steps from (25)-(30), the detection threshold and the BER can be obtained.

E. ED with Dynamic M-PSK Source

To apply ED, the PDF of received signals average energy in terms of dynamic M-PSK is required. Let $Z_{dp,i} = \frac{1}{N}\sum_{n=1}^{N}\left|y(n)|_{x=i}\right|^2$.

Theorem 2: When N is large, the PDF of $Z_{dp,i}$ is approximated as

$$p(Z_{dp,i}|x=i) = \frac{1}{\sqrt{2\pi\sigma_{dp,i}^2}} e^{-\frac{(Z_{dp,i}-\mu_{dp,i})^2}{2\sigma_{dp,i}^2}}, \tag{36}$$

where

$$\begin{aligned}\mu_{dp,i} =& z_{on}(|h_i|^2P_s+\sigma_w^2)+z_{off}\sigma_w^2,\\ \sigma_{dp,i}^2 =& \frac{2z_{on}|h_i|^2P_s\sigma_w^2+\sigma_w^4+z_{off}\sigma_w^4}{N}\\ &+\frac{z_{on}(|h_i|^2P_s+\sigma_w^2)^2-\left(z_{on}(|h_i|^2P_s+\sigma_w^2)+z_{off}\sigma_w^2\right)^2}{N}.\end{aligned} \tag{37}$$

Proof: For the M-PSK signal, the PDF of its energy conditioned on $x=i$ is approximated as [13] [32]

$$p(r_{psk,i}|x=i) = \frac{1}{\sqrt{2\pi\sigma_{psk,i}^2}} e^{-\frac{(r_{psk,i}-\mu_{psk,i})^2}{2\sigma_{psk,i}^2}}, \tag{38}$$

where

$$\begin{aligned}\mu_{psk,i} &= |h_i|^2P_s+\sigma_w^2,\\ \sigma_{psk,i}^2 &= 2|h_i|^2P_s\sigma_w^2+\sigma_w^4.\end{aligned} \tag{39}$$

Similarly, the conditional PDF of the noise signal energy is approximated by

$$p(r_{psk,w}|x=i) = \frac{1}{\sigma_w^2} e^{-\frac{r_{psk,w}}{\sigma_w^2}}, \tag{40}$$

and the mean and the variance of $r_{psk,w}$ are

$$\mu_{psk,w} = \sigma_w^2, \sigma_{psk,w}^2 = \sigma_w^4. \tag{41}$$

Then, the PDF of the received signal energy in terms of the dynamic M-PSK source is given by

$$\begin{aligned}p(r_{dp}|x=i) =& z_{on}\frac{1}{\sqrt{2\pi\sigma_{psk,i}^2}} e^{-\frac{(r_{dp}-\mu_{psk,i})^2}{2\sigma_{psk,i}^2}} +\\ & z_{off}\frac{1}{\sigma_w^2} e^{-\frac{r_{dp}}{\sigma_w^2}}.\end{aligned} \tag{42}$$

The mean of r_{dp} is derived as

$$\begin{aligned}E[r_{dp}|x=i] &= \int_{-\infty}^{+\infty} r_{dp}f(r_{dp}|x=i)dr_{dp}\\ &= z_{on}(|h_i|^2P_s+\sigma_w^2)+z_{off}\sigma_w^2.\end{aligned} \tag{43}$$

Then, the mean of r_{dp}^2 is calculated as

$$\begin{aligned}E[r_{dp}^2|x=i] =& \int_{-\infty}^{+\infty} r_{dp}^2 f(r_{dp}|x=i)dr_{dp}\\ =& 2z_{on}|h_i|^2P_s\sigma_w^2+z_{on}\sigma_w^4+z_{off}\sigma_w^4+z_{off}\sigma_w^4\\ &+z_{on}(|h_i|^2P_s+\sigma_w^2)^2.\end{aligned} \tag{44}$$

Finally, the variance of r_{dp} can be obtained by

$$\begin{aligned}&Var[r_{dp}|x=i]\\ =&E[r_{dp}^2|x=i]-(E[r_{dp}|x=i])^2\\ =&2z_{on}|h_i|^2P_s\sigma_w^2+\sigma_w^4+z_{off}\sigma_w^4\\ &+z_{on}(|h_i|^2P_s+\sigma_w^2)^2-\left(z_{on}(|h_i|^2P_s+\sigma_w^2)+z_{off}\sigma_w^2\right)^2.\end{aligned} \tag{45}$$

In summary, the mean and the variance of $Z_{dp,i}$ are given by (37). □

Following the similar steps from (25)-(30), the detection threshold and the BER can be derived.

Due to the complex PDF in (10), the truncation threshold for dynamic ambient M-PSK is intractable and truncation-aided detection methods cannot be developed. We resort to detection methods without acquiring the threshold. In the next section, we will utilize Manchester code to facilitate the detection process for the dynamic M-PSK source. Also, Manchester code is also applied to the dynamic CG source since the detection threshold is not required [13], which can make the detection more simple.

IV. Manchester Code and Detection

A typical detector for Manchester code aided ambient backscatter communication is the energy detector [13]. In this section, ED and TED are elaborated and their performance analysis is conducted.

A. ED with Dynamic CG Source

To use ED, the average energy of the received signals corresponding to two parts of the Manchester code is necessary to be determined. The PDF of the received signal energy in the half part of Manchester code can be obtained following similar derivation steps in (22)-(24) and is listed as follows

$$\bar{Z}_{dcg,i} \sim \mathcal{N}\left(\bar{\mu}_{dcg,i}, \bar{\sigma}_{dcg,i}^2\right), \tag{46}$$

where $\bar{\mu}_{dcg,i} = z_{on}\sigma_i^2 + z_{off}\sigma_w^2$ and $\bar{\sigma}_{dcg,i}^2 = \frac{\left(2z_{on}\sigma_i^4+2z_{off}\sigma_w^4-(z_{on}\sigma_i^2+z_{off}\sigma_w^2)^2\right)}{N/2}$.

The detection error at the receiver occurs when

$$\begin{cases}\bar{Z}_{dcg,1}-\bar{Z}_{dcg,0}<0, \sigma_1^2>\sigma_0^2,\\ \bar{Z}_{dcg,1}-\bar{Z}_{dcg,0}>0, \sigma_1^2<\sigma_0^2.\end{cases} \tag{47}$$

The difference of two normal random variables $\bar{Z}_{dcg,1}$ and $\bar{Z}_{dcg,0}$, also follows the normal distribution. The BER equals the probability of this difference being less than or greater than 0. Thus we have

$$\bar{P}_b^{dcg} = \frac{1}{2}erfc\left(\frac{\bar{\mu}_{dcg,1}-\bar{\mu}_{dcg,0}}{\sqrt{2(\bar{\sigma}_{Z_{dcg,1}}^2+\bar{\sigma}_{Z_{dcg,0}}^2)}}\right), \tag{48}$$

if $\sigma_1^2 > \sigma_0^2$. Similarly, we get

$$\bar{P}_b^{dcg} = \frac{1}{2} erfc\left(\frac{\bar{\mu}_{dcg,0} - \bar{\mu}_{dcg,1}}{\sqrt{2(\bar{\sigma}^2_{Z_{dcg,1}} + \bar{\sigma}^2_{Z_{dcg,0}})}}\right), \tag{49}$$

if $\sigma_0^2 > \sigma_1^2$.

Combining two cases together yields

$$\bar{P}_b^{dcg} = \frac{1}{2} erfc\left(\frac{|\bar{\mu}_{dcg,0} - \bar{\mu}_{dcg,1}|}{\sqrt{2(\bar{\sigma}^2_{Z_{dcg,1}} + \bar{\sigma}^2_{Z_{dcg,0}})}}\right). \tag{50}$$

The expression in (51) is shown at the bottom of the next page, where $\gamma = \sigma_s^2/\sigma_w^2$. When γ approaches infinity, (51) reduces to (52).

Remark 1: Since $erfc(\cdot)$ is a monotonically decreasing function and N is located in the numerator of (51), increasing N can decrease the BER constantly. Besides, in the infinite SNR region, z_{on} still has an impact on the BER which can be observed from (52). That is, increasing z_{on} leads to a decrease in the BER. Moreover, (52) indicates that there is a BER error floor in the high SNR level for dynamic complex Gaussian sources. The situation is reasonable since there is a BER error floor for static complex Gaussian sources and dynamic complex Gaussian sources are more complex than static ones.

B. TED with Dynamic CG Source

The receiver needs to truncate the received signals in both two parts of Manchester code using the truncation threshold T_s. The theoretical number of residual signals after truncation is

$$\begin{aligned}\bar{N}_{on,i} &= N \cdot p(r(n) > T_s) \\ &= N\left(z_{on} e^{-\frac{T_s}{\sigma_i^2}} + z_{off} e^{-\frac{T_s}{\sigma_w^2}}\right).\end{aligned} \tag{53}$$

The average energy of the residual signals is calculated by

$$\bar{Z}^t_{dcg,i} = \frac{1}{\bar{N}_{on,i}} \sum_{n=1}^{\bar{N}_{on,i}} \left|y_t(n)|_{x=i}\right|^2. \tag{54}$$

Following the steps in (31)-(35), the PDFs of $\bar{Z}^t_{dcg,i}$ are

$$\bar{Z}^t_{dcg,0} \sim \mathcal{N}\left(\frac{z_{on}(T_s+\sigma_0^2)e^{-\frac{T_s}{\sigma_0^2}} + z_{off}(T_s+\sigma_w^2)e^{-\frac{T_s}{\sigma_w^2}}}{z_{on}e^{-\frac{T_s}{\sigma_0^2}} + z_{off}e^{-\frac{T_s}{\sigma_w^2}}}, \frac{Var[r|x=0]}{\bar{N}_{on,0}}\right), \tag{55}$$

$$\bar{Z}^t_{dcg,1} \sim \mathcal{N}\left(\frac{z_{on}(T_s+\sigma_1^2)e^{-\frac{T_s}{\sigma_1^2}} + z_{off}(T_s+\sigma_w^2)e^{-\frac{T_s}{\sigma_w^2}}}{z_{on}e^{-\frac{T_s}{\sigma_1^2}} + z_{off}e^{-\frac{T_s}{\sigma_w^2}}}, \frac{Var[r|x=1]}{\bar{N}_{on,1}}\right). \tag{56}$$

The BER is calculated as

$$\bar{P}_b^{t,dcg} = \frac{1}{2} erfc\left(\frac{|\bar{\mu}^t_{dcg,0} - \bar{\mu}^t_{dcg,1}|}{\sqrt{2((\bar{\sigma}^t_{dcg,1})^2 + (\bar{\sigma}^t_{dcg,0})^2)}}\right). \tag{57}$$

where $\bar{\mu}^t_{dcg,i} = \frac{z_{on}(T_s+\sigma_i^2)e^{-\frac{T_s}{\sigma_i^2}} + z_{off}(T_s+\sigma_w^2)e^{-\frac{T_s}{\sigma_w^2}}}{z_{on}e^{-\frac{T_s}{\sigma_i^2}} + z_{off}e^{-\frac{T_s}{\sigma_w^2}}}$, and $(\bar{\sigma}^t_{dcg,i})^2 = \frac{Var[r|x=i]}{\bar{N}_{on,i}}$.

C. ED with Dynamic M-PSK Source

Let $\bar{Z}_{dp,i} = \frac{2}{N}\sum_{n=1}^{N/2}\left|y(n)|_{x=i}\right|^2$ denote the average energy of the received signal under the dynamic M-PSK source. When $N/2$ is large, the PDF of $\bar{Z}_{dp,i}$ is derived approximately as

$$p(\bar{Z}_{dp,i}|x=i) = \frac{1}{\sqrt{2\pi\bar{\sigma}^2_{dp,i}}} e^{-\frac{(Z-\bar{\mu}_{dp,i})^2}{2\bar{\sigma}^2_{dp,i}}}, \tag{58}$$

where

$$\begin{aligned}\bar{\mu}_{dp,i} =& z_{on}(|h_i|^2 P_s + \sigma_w^2) + z_{off}\sigma_w^2, \\ \bar{\sigma}^2_{dp,i} =& \frac{2z_{on}|h_i|^2 P_s\sigma_w^2 + \sigma_w^4 + z_{off}\sigma_w^4}{N/2} \\ &+ \frac{z_{on}(|h_i|^2 P_s+\sigma_w^2)^2 - \left(z_{on}(|h_i|^2 P_s+\sigma_w^2)+z_{off}\sigma_w^2\right)^2}{N/2}.\end{aligned} \tag{59}$$

The BER is shown in (60) at the top of the next page. In the asymptotic high SNR regime, (60) is degenerated to

$$\bar{P}_b^{dcg} = \frac{1}{2} erfc\left(\frac{\sqrt{N}|z_{on}(|h_0|^2 - |h_1|^2)|}{2\sqrt{2z_{on}(|h_1|^2+\frac{1}{\gamma})^2 + 2z_{on}(|h_0|^2+\frac{1}{\gamma})^2 + \frac{4z_{off}}{\gamma^2} - \left(z_{on}^2(|h_1|^2+\frac{1}{\gamma})^2 + \frac{z_{off}^2}{\gamma^2} + 2z_{on}z_{off}(\frac{|h_1|^2}{\gamma}+\frac{1}{\gamma^2})\right) - \left(z_{on}^2(|h_0|^2+\frac{1}{\gamma})^2 + \frac{z_{off}^2}{\gamma^2} + 2z_{on}z_{off}(\frac{|h_0|^2}{\gamma}+\frac{1}{\gamma^2})\right)}}\right). \tag{51}$$

$$\tilde{P}_b^{dcg} = \frac{1}{2} erfc\left(\frac{\sqrt{N}|z_{on}(|h_0|^2 - |h_1|^2)|}{2\sqrt{2z_{on}|h_1|^4 + 2z_{on}|h_0|^4 - z_{on}^2(|h_1|^2)^2 - z_{on}^2(|h_0|^2)^2}}\right). \tag{52}$$

This article has been accepted for publication in IEEE Transactions on Communications. This is the author's version which has not been fully edited and content may change prior to final publication. Citation information: DOI 10.1109/TCOMM.2025.3548758

$$\tilde{P}_b^{dp}=\frac{1}{2}erfc\left(\frac{\sqrt{N}\left|z_{on}(|h_0|^2-|h_1|^2)\right|}{2\sqrt{2z_{on}|h_1|^2\frac{1}{\gamma}+\frac{2}{\gamma^2}+\frac{2z_{off}}{\gamma^2}+z_{on}\left(|h_1|^2+\frac{1}{\gamma}\right)^2-\left(z_{on}|h_1|^2+\frac{1}{\gamma}\right)^2+2z_{on}|h_0|^2\frac{1}{\gamma}+z_{on}\left(|h_0|^2+\frac{1}{\gamma}\right)^2-\left(z_{on}|h_0|^2+\frac{1}{\gamma}\right)^2}}\right). \quad (60)$$

$$\tilde{P}_b^{dp}=\frac{1}{2}erfc\left(\frac{\sqrt{N}|z_{on}(|h_0|^2-|h_1|^2)|}{2\sqrt{z_{on}|h_1|^4-\left(z_{on}|h_1|^2\right)^2+z_{on}|h_0|^4-\left(z_{on}|h_0|^2\right)^2}}\right). \quad (61)$$

Remark 2: Similar to the analysis in *Remark 1*, increasing N can decrease the BER constantly and increasing z_{on} leads to the decrease of the BER. Furthermore, (61) indicates that there is a BER error floor in the high SNR level for dynamic M-PSK sources. This result is different from existing works on static M-PSK sources since there is no BER error floor for static ones.

D. TED with Dynamic M-PSK Source

Although the truncation threshold is intractable for the M-PSK source, the detection of truncated energy can be achieved by throwing away the same number of the received signals in two parts of Manchester code. Specifically, we can sort the received signal energy values in the ascending order for each part of Manchester code. Then, the first N_{trun} signals from both two parts of Manchester code are discarded. After truncating part of received signals, the symbol detection is performed by comparing the first and second half received signals energy level.

V. Simulation Results and Discussions

In this section, simulation results are presented to evaluate the performance of the proposed schemes.

We set $h_d \sim \mathcal{CN}(0,10)$, $h_b, h_f \sim \mathcal{CN}(0,1)$. The coefficient α representing the scattering efficiency and antenna gain is 0.5. The probability of the source in the on-state is z_{on} is 0.8, unless stated otherwise. The source power σ_s^2 and P_s are equal and set to be 1 and the SNR is defined as σ_s^2/σ_w^2. The symbol duration ratio between the tag and the source is $N = 100$, unless stated otherwise. The type of the M-PSK source is the binary-PSK source without loss of generality.

A. BER of OOK Modulation under Dynamic Sources

First, the BER of the OOK modulation with both the dynamic CG source and the M-PSK source is illustrated in Fig. 2. The theoretical analysis is consistent with the simulations results. This is because when N is sufficiently large, the Gaussian distribution approximates the exact PDF well. For the dynamic CG source, TED outperforms ED in the high SNR region since TED truncates some noise signals. In the low SNR region, TED may truncate some useful signals since the noise level is high. As for the LRT detection, it always has a better performance than TLRT since it obeys the ML

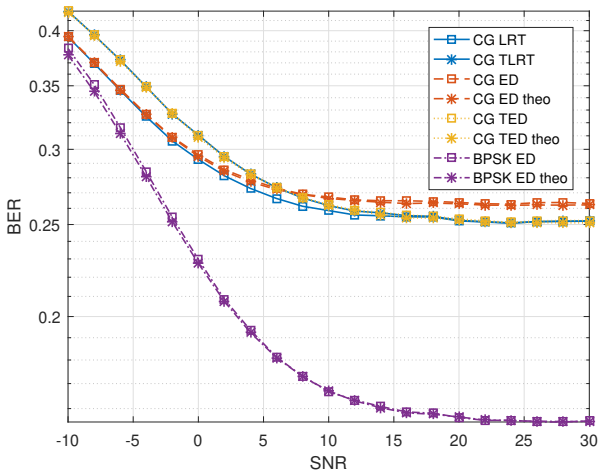

Fig. 2. BER versus SNR of the OOK modulation

principle. Also, it has a lower BER than ED and TED. In the high SNR region, TED achieves almost the same BER compared with LRT. The BER under the BPSK source is much lower than the BER of the CG source due to BPSK signals' constant envelope. With the increase of the SNR, all BERs decrease. Moreover, all BER curves meet an error floor when the SNR is large. In the previous works, we know only the BER with the CG source has an error floor while the BER with a constantly-transmitting M-PSK source does not [11]–[13]. Due to the pure noise signals in the received signals, the BER of the dynamic M-PSK source also has an error floor.

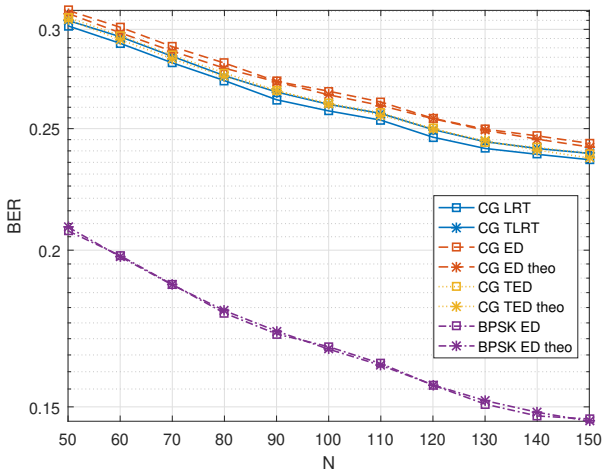

Fig. 3. BER versus N of the OOK modulation

Then, we study the impact of N and z_{on} on the BER

This article has been accepted for publication in IEEE Transactions on Communications. This is the author's version which has not been fully edited and content may change prior to final publication. Citation information: DOI 10.1109/TCOMM.2025.3548758

performance. The SNR is set as 10 dB.

The BER of the OOK modulation with both the CG source and the M-PSK source versus N is shown in Fig. 3. For both two sources, the BER decreases when N increases and there is no error floor when N is large. This phenomenon reminds us to increase N for decreasing the BER.

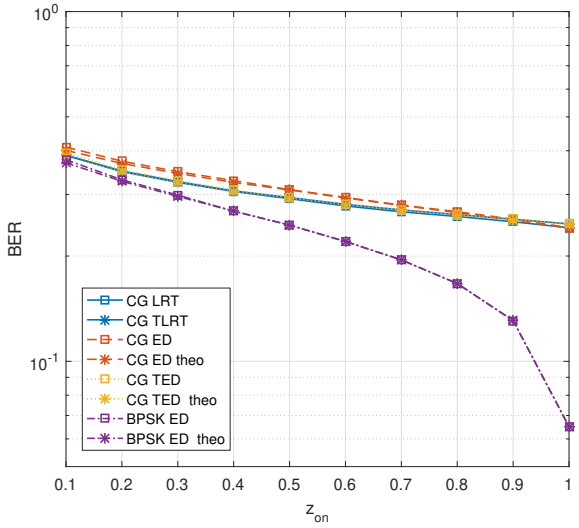

Fig. 4. BER versus z_{on} of the OOK modulation

Fig. 4 presents the impact of z_{on} on the BER of the OOK modulation with both the dynamic CG source and the M-PSK source. For both two sources, the BER decreases when z_{on} increases and does not have an error floor when z_{on} is large. This is because the increase of z_{on} does not increase the source signal strength but increase the amount of received information signals. Specifically, when z_{on} increases, the gaps between different detectors for the dynamic CG source become narrow. This trend indicates that the low complexity ED is desirable when z_{on} approaches 1. Moreover, when z_{on} approximately equals 1, the ED has a better BER performance than TED since there is few pure noise signals. It is undesirable to truncate received signals under this situation.

B. BER of Manchester Code under Dynamic Sources

The BER of Manchester code with both the dynamic CG source and the M-PSK source versus the SNR is illustrated in Fig. 5. The BER under the CG source is higher than the BER under the M-PSK source since the CG signal is more complex than the M-PSK signal. For both two sources, the TED detector outperforms the ED detector when the SNR is high. Specifically, under the BPSK source, TED has a lower BER across the whole SNR axis.

Fig. 6 shows the BER of Manchester code with both the dynamic CG source and the M-PSK source versus N. For both two sources, the BER decreases with increasing N and there is no error floor when N is large. This is consistent with the equations in (51) and (60). The function $erfc(\cdot)$ is a monotonically decreasing and N is located in the numerator. It is significant to increase the value of N to decrease the BER continuously.

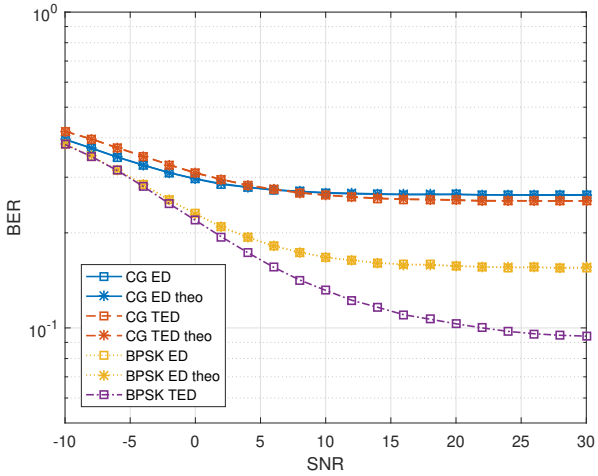

Fig. 5. BER versus SNR of Manchester code

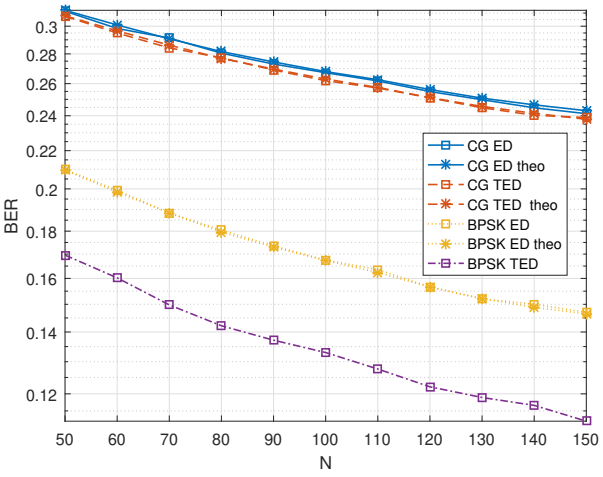

Fig. 6. BER versus N of Manchester code

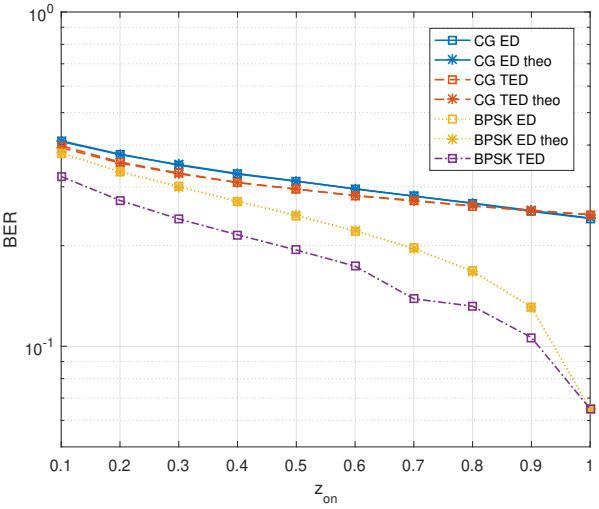

Fig. 7. BER versus z_{on} of Manchester code

Fig. 7 presents the BER of Manchester code with both the CG source and the M-PSK source versus z_{on}. The BER decreases when z_{on} increases and there is no error floor when z_{on} is high. Specifically, with z_{on} increases, the gaps between different detectors of the same type of signal become narrow. When z_{on} approaches 1, the ED has a better BER performance than TED since TED truncates some useful signals in this situation.

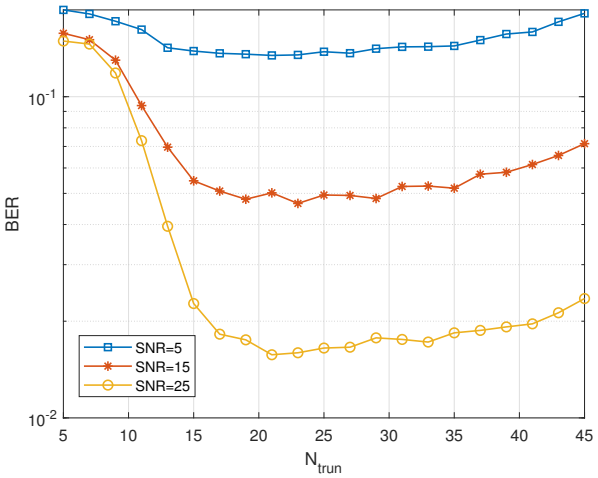

Fig. 8. BER versus N_{trun} of Manchester code with TED under the dynamic M-PSK source.

Finally, the impact of the number of truncated signals with the TED detector under the BPSK source on BER is investigated. When N_{trun} is small, the BER decreases with the increase of N_{trun}. This is because with the increase of N_{trun}, more noise signals can be removed. Besides, the optimal N_{trun} increases with SNR. When N_{trun} is large enough, the BER does not decrease. The reason is that a large N_{trun} leads to the discarding of useful signals. Moreover, if N_{trun} is too large, the BER will increase. Thus, the amount of received signals to be discarded should be chosen properly.

In summary, the AmBC system has a better BER performance under the PSK sources compared to the CG sources. The LRT detection has a lower BER than ED. The truncation based detection outperforms the non-truncation method in the high SNR regime. There is no BER error floor with a large N or z_{on} level while such floor exists with a high SNR for both two types of sources.

VI. Conclusion

In this paper, we studied the detections of ambient backscatter communication under dynamic sources. We develop detection methods with/without truncating signals for AmBC under dynamic CG signals with the OOK modulation. Manchester code can be applied to make the detection more simple and tractable for dynamic M-PSK. This code does not need to estimate the detection threshold. Moreover, the energy truncation threshold is not explicitly required with Manchester code for dynamic M-PSK. Instead, only the number of truncated received signals is required. Simulation results shows it is necessary to truncate part of signals in detections in the high SNR region when the probability of the source on is not close to 1. Both BERs of the dynamic CG and dynamic M-PSK source meet an error floor under the high SNR situation while such error floor disappears when increasing the symbol duration ratio between the tag and the source.

As our future work, we will further extend our detection method to the PSK modulated tag.

References

[1] N. Van Huynh, D. T. Hoang, X. Lu, D. Niyato, P. Wang, and D. I. Kim, "Ambient backscatter communications: A contemporary survey," *IEEE Commun. Surveys Tuts.*, vol. 20, no. 4, pp. 2889–2922, 4th Quart., 2018.

[2] C. Xu, L. Yang and P. Zhang, "Practical backscatter communication systems for battery-free Internet of Things: A tutorial and survey of recent research," *IEEE Signal Process. Mag.*, vol. 35, no. 5, pp. 16-27, Sep. 2018.

[3] B. Gu, D. Li, H. Ding, G. Wang and C. Tellambura,"Breaking the Interference and Fading Gridlock in Backscatter Communications: State-of-the-Art, Design Challenges, and Future Directions," *IEEE Commun. Surveys Tut.*, early access, 2024.

[4] T. Jiang, Y. Zhang, W. Ma, M. Peng, Y. Peng, M. Feng and G. Liu, "Backscatter communication meets practical battery-free Internet of Things: A survey and outlook," *IEEE Commun. Surv. Tuts.*, vol. 25, no. 3, pp. 2021–2051, 3rd-quarter, 2023.

[5] V. Liu, A. Parks, V. Talla, S. Gollakota, D. Wetherall, and J. R. Smith, "Ambient backscatter: Wireless communication out of thin air," in *Proc. ACM SIGCOMM*, Jun. 2013, pp. 39-50.

[6] A. Wang, V. Iyer, V. Talla, J. R. Smith, and S. Gollakota, "FM backscatter: Enabling connected cities and smart fabrics," in *Proc. 14th USENIX Symp. Netw. Syst. Design Implement. (NSDI)*, 2017, pp. 243–258.

[7] Y. Chen, A. A. Khuwaja, C.-X. Wang, "Effect of Source Signal Traffic on Signal Detection for Ambient Backscatter Communication," *IEEE Trans. Veh. Technol.*, vol. 73, no. 11, pp. 16790-16804, Nov. 2024.

[8] S. Abdallah, A. I. Salameh, M. Saad and M. A Albreem, "Asynchronous Ambient Backscatter Communication Systems: Joint Timing Offset and Channel Estimation," *IEEE Trans. Commun.*, early access, pp. 1-15, Apr. 2024.

[9] W. Liu, S. Shen, D. H. K. Tsang, and R. D. Murch, "Enhancing ambient backscatter communication utilizing coherent and non-coherent space-time codes," *IEEE Trans. Wireless Commun.*, vol. 20, pp. 6884–6897, Oct. 2021.

[10] D. Li, "Two birds with one stone: Exploiting decode-and-forward relaying for opportunistic ambient backscattering," *IEEE Trans. Commun.*, vol. 68, no. 3, pp. 1405-1416, Mar. 2020.

[11] J. Qian, F. Gao, G. Wang, S. Jin, and H. Zhu, "Noncoherent detections for ambient backscatter system," *IEEE Trans. Wireless Commun.*,vol. 16, no. 3, pp. 1412–1422, Mar. 2017.

[12] J. Qian, F. Gao, G. Wang, S. Jin, and H. Zhu, "Semi-coherent detection and performance analysis for ambient backscatter system," *IEEE Trans. Commun.*, vol. 65, no. 12, pp. 5266–5279, Dec. 2017.

[13] Q. Tao, C. Zhong, H. Lin, and Z. Zhang, "Symbol detection of ambient backscatter systems with Manchester coding," *IEEE Trans. Wireless Commun.*, vol. 17, no. 6, pp. 4028–4038, 2018.

[14] J. K. Devineni and H. S. Dhillon, "Non-coherent detection and bit error rate for an ambient backscatter link in time-selective fading," *IEEE Trans. Commun.*, vol. 69, no. 1, pp. 602-618, Jan. 2021.

[15] S. Guruacharya, X. Lu and E. Hossain, "Optimal non-coherent detector for ambient backscatter communication system," *IEEE Trans. Veh. Technol.*, vol. 69, no. 12, pp. 16197-16201, Dec. 2020.

[16] Q. Tao, C. Zhong, X. Chen, H. Lin and Z. Zhang, "Maximum-eigenvalue detector for multiple antenna ambient backscatter communication systems," *IEEE Trans. Veh. Technol.*, vol. 68, no. 12, pp. 12411-12415, Dec. 2019.

[17] Q. Tao, C. Zhong, X. Chen, H. Lin and Z. Zhang, "Optimal detection for ambient backscatter communication systems with multiantenna reader under complex Gaussian illuminator," *IEEE Internet Things J.*, vol. 7, no. 12, pp. 11371-11383, Dec. 2020.

[18] G. Wang, F. Gao, R. Fan and C. Tellambura, "Ambient backscatter communication systems: detection and performance analysis," *IEEE Trans. Commun.*, vol. 64, no. 11, pp. 4836-4846, Nov. 2016.

[19] K. Lu, G. Wang, F. Qu and Z. Zhong, "Signal detection and BER analysis for RF-powered devices utilizing ambient backscatter," *Proc. IEEE Int. Conf. Wireless Commun. Signal Process. (WCSP)*, pp. 1-5, Oct. 2015.

[20] Y. Chen and W. Feng, "Novel signal detectors for ambient backscatter communications in Internet of Things applications," *IEEE Internet of Things J.*, vol. 11, no. 3, pp. 5388-5400, Aug. 2024.

[21] Q. Tao, C. Zhong, K. Huang, X. Chen and Z. Zhang, "Ambient backscatter communication systems with MFSK modulation," *IEEE Trans. Wireless Commun.*, vol. 18, no. 5, pp. 2553-2564, May 2019.

[22] D. Darsena, G. Gelli and F. Verde, "Modeling and performance analysis of wireless networks with ambient backscatter devices," *IEEE Trans. Commun.*, vol. 65, no. 4, pp. 1797-1814, Apr. 2017.

[23] J. Qian, Y. Zhu, C. He, F. Gao and S. Jin, "Achievable rate and capacity analysis for ambient backscatter communications," *IEEE Trans. Commun.*, vol. 67, no. 9, pp. 6299-6310, Sept. 2019.

[24] W. Zhao, G. Wang, R. Fan, L. S. Fan and S. Atapattu, "Ambient backscatter communication systems: Capacity and outage performance analysis," *IEEE Access*, vol. 6, no. 1, pp. 22695-22704, 2018.

[25] X. He, W. Jiang, M. Cheng, X. Zhou, P. Yang, and B. Kurkoski, "Guardrider: Reliable WiFi backscatter using Reed-Solomon codes with QoS guarantee," in *IEEE/ACM IWQoS*, June 2020, pp. 1–10.

[26] P. Li, X. He, N. M. Freris and P. Yang. "Capacity analysis of ambient backscatter system with Bernoulli distributed excitation" in *Wireless Algorithms, Systems, and Applications (WASA): 15th International Conference,* Sept. 2020, pp. 1-13.

[27] J. Chen, H. Yu, Q. Guan, G. Yang, and Y.-C. Liang, "Achievable rate and capacity analysis for ambient backscatter communications with dynamic sources," in *Proc. IEEE VTC-Fall*, Sept. 2022, pp. 1-5.

[28] J. Qian, A. N. Parks, J. R. Smith, F. Gao and S. Jin, "IoT communications with M-PSK modulated ambient backscatter: Algorithm analysis and implementation", *IEEE Internet Things J.*, vol. 6, no. 1, pp. 844-855, Feb. 2019.

[29] B. Kellogg, A. Parks, S. Gollakota, J. R. Smith and D. Wetherall, "Wi-Fi backscatter: Internet connectivity for RF-powered devices," in *Proc. ACM SIGCOMM*, Aug. 2014, pp. 607-618.

[30] R. J. Pirkl, "Moments of the truncated complex Gaussian distribution," *Nat. Inst. Standards and Technol., Boulder CO NIST Tech. Note 1560 Tech. Rep*, 2011.

[31] R. Kan and C. Robotti, "On moments of folded and truncated multivariate normal distributions," *J. Comput. Graphical Statist.*, vol. 26, no. 4, pp. 930-934, 2017.

[32] J. G. Proakis, *Digital Communications*, 5th ed. New York, NY, USA: McGraw-Hill, 2007.

Jixiang Chen received the B.S. degree from Fuzhou University, Fuzhou, China, in 2019, and is pursuing a Ph.D. degree with the South China University of Technology, Guangzhou, China. He is currently a visiting student at Curtin University, Perth, Australia. His research interests include backscatter communications, performance analysis, modulation, and detection.

Quansheng Guan (S'09-M'11-SM'17) received the Ph.D. degree from South China University of Technology (SCUT), Guangzhou, China, in 2011. From 2009 to 2010, he was a visiting Ph.D. student with the University of British Columbia, Vancouver, Canada. From 2012 to 2013, he was a Postdoc Researcher at the Chinese University of Hong Kong, Hong Kong. He was a visiting scholar at Singapore University of Technology and Design, Singapore, in 2013, and a visiting professor in Polytech Nantes, Nantes, France, in 2016. He is currently a full Professor with the School of Electronic and Information Engineering, SCUT. His main research interests are in the areas of wireless networks, underwater acoustic networks, cloud/fog computing, as well as integrated sensing and communications.

Dr. Guan is the co-recipients of Best Paper Awards from IEEE ICCC 2014, IEEE ICNC 2016 and ACPEE 2023, and the Best Demo Award from ACM WUWNET 2018. He was a guest editor for Mobile Information System. He is associate editors for IEEE Access and International Journal of Distributed Sensor Networks.

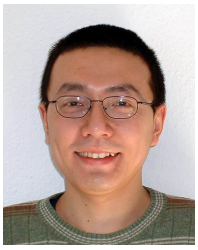

Yue Rong (Senior Member, IEEE) received the Ph.D. degree (summa cum laude) in electrical engineering from Darmstadt University of Technology, Darmstadt, Germany, in 2005.

He was a Postdoctoral Researcher with the Department of Electrical Engineering, University of California at Riverside, Riverside, CA, USA, from February 2006 to November 2007. Since December 2007, he has been with Curtin University, Bentley, WA, Australia, where he is currently a Professor. His research interests include signal processing for communications, underwater acoustic communications, underwater optical wireless communications, machine learning, speech recognition, and biomedical engineering. He has published over 200 journal and conference papers in these areas.

Prof. Rong was a Senior Area Editor of the IEEE TRANSACTIONS ON SIGNAL PROCESSING from 2020 to 2024. He was an Editor of the IEEE WIRELESS COMMUNICATIONS LETTERS from 2012 to 2014 and a Guest Editor of the IEEE JOURNAL ON SELECTED AREAS IN COMMUNICATIONS Special Issue on Theories and Methods for Advanced Wireless Relays. He was an Associate Editor of the IEEE TRANSACTIONS ON SIGNAL PROCESSING from 2014 to 2018.

Hua Yu (Member, IEEE) received the B.S. degree in mathematics from Southwest University, Chongqing, China, in 1995, and the Ph.D. degree in communication and information system from South China University of Technology, Guangzhou, China, in 2004. From 2012 to 2013, he was a Visiting Scholar with the School of Marine Science and Policy, University of Delaware, Newark, DE, USA. He is currently a Professor with the School of Electronic and Information Engineering, South China University of Technology; and an Adjunct Researcher with the Key Laboratory of Marine Environmental Survey Technology and Application, Ministry of Natural Resources, Guangzhou. He is also the Director of the Department of Underwater Communications, National Engineering Technology Research Center for Mobile Ultrasonic Detection. His main research interests include the areas of wireless communications, underwater acoustic communications, and networks. Dr. Yu was a co-recipient of the Best Paper Award from IEEE ICNC 2016 and the Best Demo Award from ACM WUWNET 2018.